Structure refinement of the icosahedral AlPdMn quasicrystal using quantitative convergent beam electron diffraction and symmetry-adapted parameters

2003 J. Phys.: Condens. Matter 15 4947

(http://iopscience.iop.org/0953-8984/15/29/306)

INSTITUTE OF PHYSICS PUBLISHING JOURNAL OF PHYSICS: CONDENSED MATTER

J. Phys.: Condens. Matter **15** (2003) 4947–4960 PII: S0953-8984(03)59829-0

Structure refinement of the icosahedral AlPdMn quasicrystal using quantitative convergent beam electron diffraction and symmetry-adapted parameters

Aihua Fang[1], **Huamin Zou**[1,2,4], **Fengmei Yu**[1], **Renhui Wang**[1,2] **and Xiaofeng Duan**[3]

[1] Department of Physics, Wuhan University, Wuhan 430072, China
[2] Centre for Electron Microscopy, Wuhan University, Wuhan 430072, China
[3] Beijing Laboratory of Electron Microscopy, Institute of Physics and Centre for Condensed Matter Physics, Chinese Academy of Sciences, Beijing 100080, China

E-mail: hmzou@whu.edu.cn

Received 20 February 2003, in final form 13 June 2003
Published 11 July 2003
Online at stacks.iop.org/JPhysCM/15/4947

Abstract

The atomic structure of the perfect AlPdMn icosahedral phase has been studied on a single-crystal specimen using the quantitative convergent beam electron diffraction (QCBED) technique combined with a description of the shapes of atomic surfaces using a symmetry-adapted series of surface harmonics. The spherical model (Boudard *et al* 1992 *J. Phys.: Condens. Matter* **4** 10149) was used as a starting point for the refinement. By fitting the calculated electron diffraction intensities in the CBED line profile to the experimental electron diffraction intensities, the coefficients in the surface harmonic expansion of the atomic surfaces' boundaries are refined. The refined parameters show that the fluctuations of the external boundary of atomic surface for Pd at n_0 can be as large as 0.2 nm. The boundaries of the atomic surfaces for Mn show little fluctuation. Compared to the spherical model, in the present model the number of unphysically short interatomic distances is reduced significantly. The three-dimensional atomic clusters with centres located successively at the six-dimensional lattice nodes n_0, n_1 and bc_1 are generated by means of the cut method.

1. Introduction

Quasicrystals represent a form of matter that differs from the other two forms—crystalline and amorphous—by possessing quasiperiodic translational order and non-crystallographic

[4] Author to whom any correspondence should be addressed.

orientational order. The atomic structure of quasicrystals is now mostly understood through high-dimensional crystallography. In this scheme the periodicity is recovered in a six-dimensional (6D) space for structures that present icosahedral symmetry. The periodic space decomposes into two subspaces: the parallel space (physical space) and the perpendicular space. In the cut scheme, the atomic structure is described by a set of atomic surfaces (atomic hypersurfaces or atomic occupation domains) which extend in the perpendicular space and decorate the higher-dimensional unit cell. For the case of icosahedral phases, the atomic surfaces are three-dimensional objects. To solve the structure of a quasicrystal, one must determine both the positions and the shapes of the atomic surfaces.

Boudard *et al* [1] proposed a spherical model to describe the atomic structure of icosahedral AlPdMn quasicrystals based on their neutron and x-ray single-crystal studies. In this model, the icosahedral AlPdMn phase has a face-centred hypercubic lattice and the atomic surfaces are either spheres or spherical shells. The atomic surfaces are located on three special positions of the hypercubic unit cell: (i) three successive shells located on $n_0 = [000000]$—the spherical core of Mn, an intermediate shell of Pd and an outer shell of Al; (ii) two successive shells located on $n_1 = \frac{1}{2}[100000]$—the core of Mn and an outer shell of Al; and (iii) a ball of Pd located on $bc_1 = \frac{1}{4}[11111\bar{1}]$. Although the shapes of the atomic surfaces are simple, this model produces quite well the x-ray diffraction intensities of the strongest reflections which correspond to the reflections with small perpendicular components, $\boldsymbol{g}^{\mathrm{perp}}$, of the 6D reciprocal vectors. This is because, in the low-$\boldsymbol{g}^{\mathrm{perp}}$ region, the Fourier transform of the atomic surfaces is mainly sensitive to their sizes and not their precise shapes. Later, de Boissieu *et al* [2] found, according to their anomalous x-ray diffraction study, that the geometrical irregularity of the atomic surface that describes the Pd atoms is of the order of 0.1 nm. To refine the atomic structure of icosahedral quasicrystal $Al_{57}Li_{32}Cu_{11}$, Elcoro *et al* [3, 4] used symmetry-adapted surface harmonics to describe the boundaries of atomic surfaces in perpendicular space and performed the refinement on neutron and x-ray diffraction data.

The shapes of atomic surfaces are directly related to the local arrangement of atoms. The magnitude and phase of a structure factor also depend on the arrangement of the atoms. In electron diffraction, the dynamical effect is very strong and the intensities of diffraction beams can be calculated precisely using the dynamical theory of electron diffraction. Thus, the quantitative convergent beam electron diffraction (QCBED) technique can be employed to determine the structure factors of crystals to an accuracy of 0.1% in magnitude and 0.1° in phase [5]. Such a feature can be helpful in determining the shapes of atomic surfaces. In addition, convergent beam electron diffraction (CBED) can provide information from a perfect micro-area as small as 1 nm in diameter, so that the influence of defects in quasicrystals is minimized. The purpose of this paper is to get more information about the shapes of the atomic surfaces of icosahedral AlPdMn quasicrystals by means of the QCBED technique combined with the surface harmonic description of the shape of the atomic surface.

2. Experimental details

Large single-quasicrystal samples of $Al_{70.5}Pd_{21}Mn_{8.5}$ were kindly provided by Professor K Urban of the Institute for Solid State Research, Research Center Juelich GmbH, Germany. These single quasicrystals were grown by using the Czochralski method. The specimen for transmission electron microscopy observation was prepared by the standard method, mechanical thinning and finally ion milling. The CBED experiments were performed using a Philips CM200-FEG microscope equipped with a Gatan image filter (GIF) and a Gatan 1024×1024 pixel slow-scan CCD camera in the Beijing Laboratory of Electron Microscopy. During the experiments, the Gatan double-tilt specimen holder was cooled with liquid nitrogen.

The temperature in the specimen was lower than −150 °C. An energy window of 10 eV around the zero-loss energy was elected. To avoid the influence of defects and obtain structural information from a region as perfect as possible, a nominal size of electron probe (1.2 nm) was used. This choice was also made on the basis of the following facts. First, since the thickness of a specimen for transmission electron microscopy is about 100 nm, a large number of atoms—which the incident electrons meet on their way through the specimen—scatter the electrons coherently. Second, among the spacings corresponding to 329 reflections in the x-ray diffraction of a single quasicrystal [2], the largest plane spacing is 0.889 nm ($2\pi/d = 7.07\ \mathrm{nm}^{-1}$). The probe size of 1.2 nm is larger than all the spacings corresponding to those reflections with measurable intensities. Third, for case of the coherent electron beam, if the probe size is less than the lattice plane spacing, then the CBED pattern depends on the probe position [8]. When we took one CBED pattern after another at the 'same' point and with the same experiment conditions, the location of the electron probe was actually different due to the drift of the specimen. However, no difference was observed from such CBED patterns. This indicates that the size of the electron probe is larger than the spacings of the planes that can give significant reflections. The accelerating voltage was 195.35 kV, which was obtained by fitting the dynamically simulated CBED pattern to the experimental pattern taken from a single-crystal specimen of silicon.

3. Structure refinement

3.1. Calculation of diffraction intensities for icosahedral AlPdMn quasicrystals

Since the diffraction peaks of quasicrystals are densely distributed in diffraction space, an overlap of diffraction disks is unavoidable for quasicrystals. However, as has been proved by Tanaka *et al* [6], if the electron beam is focused onto the specimen, the intensity at the overlapping region becomes uniform and equals the sum of the intensities of the two overlapping disks plus a constant term. Also, this constant term becomes zero when the beam size is larger than the lattice spacing. In the present simulation, the positions of disks are calculated and the intensities for individual disks at the overlapping region are summed.

The wave-mechanical formulation of electron diffraction dynamical theory for classical crystals can be applied to quasicrystals [7], provided that V_g, the Fourier components of the potential $V(\boldsymbol{r})$, are defined as

$$V_g = [h^2/(2me)]U_g = [h^2/(2me)]S(\boldsymbol{g}^{\mathrm{par}})/(\pi V). \tag{1}$$

Here $S(\boldsymbol{g}^{\mathrm{par}})/V$ is the scattering power per unit volume of the quasicrystal for $\boldsymbol{g}^{\mathrm{par}}$, the parallel subspace component of the 6D reciprocal vector $\boldsymbol{g}$. The problem is then reduced to solving the standard dispersion equation for CBED [8]:

$$\frac{(2KS_g + \mathrm{i}U'_0)B_g^{(j)}}{1 + g_n^{\mathrm{par}}/K_n} + \sum_{h\neq g} \frac{(U_{g-h} + \mathrm{i}U'_{g-h})B_h^{(j)}}{\sqrt{1 + g_n^{\mathrm{par}}/K_n}\sqrt{1 + h_n^{\mathrm{par}}/K_n}} = 2K_n\gamma^{(j)}B_g^{(j)} \tag{2}$$

and

$$B_g^{(j)} = (1 + g_n^{\mathrm{par}}/K_n)^{1/2}C_g^{(j)}. \tag{3}$$

Here, g_n^{par} is the component of $\boldsymbol{g}^{\mathrm{par}}$ along the normal of the specimen surface, S_g is the deviation parameter of the $\boldsymbol{g}^{\mathrm{par}}$ reflection, and $\boldsymbol{K}$ is the refraction-corrected wavevector. The anomalous absorption has been considered by introducing the imaginary part U'_g to the potential in equation (2). For the case that there is no inversion centre, both U_g and U'_g are complex. The solution of equation (2) then gives the generally complex $\gamma^{(j)}$ and $C_g^{(j)}$. Finally, the intensity for a given incident beam direction can be calculated as usual:

$$I_g(\boldsymbol{K}) = \left| \sum_i C_0^{-1^{(i)}} C_g^{(i)} \exp(2\pi \mathrm{i} \gamma^{(i)} t) \right|^2. \tag{4}$$

In equation (4), t is the thickness of the specimen and $C_0^{-1^{(i)}}$ is the ith element in the column, corresponding to the transmitted beam, of the inverse of the matrix whose elements are $C_g^{(i)}$ (rows i, columns g).

In calculating the structure factor for quasicrystals, the summation over points in the unit cell, as in the case of the classic crystal, must be replaced by integration over the atomic surfaces followed by a summation over these surfaces in the superspace unit cell. Therefore, the structure factor can be expressed as [9]

$$F_G = \sum_{j=1}^{m} T_j(\boldsymbol{g}^{\mathrm{par}}, \boldsymbol{g}^{\mathrm{perp}}) f_j(g^{\mathrm{par}}) q_j(\boldsymbol{g}^{\mathrm{perp}}) \exp(2\pi \mathrm{i} \boldsymbol{G} \cdot \boldsymbol{R}_j), \tag{5}$$

where $T_j(\boldsymbol{g})$ is the temperature factor. It is assumed here that a single thermal tensor $\boldsymbol{B}_j$ is associated with all the atoms represented by the points in one atomic surface and thus independent from $\boldsymbol{r}^{\mathrm{perp}}$. Here, $\boldsymbol{r}^{\mathrm{par}}$ and $\boldsymbol{r}^{\mathrm{perp}}$ are components of the 6D vector $\boldsymbol{R}$ in the parallel and perpendicular subspaces, respectively. For the icosahedral AlPdMn quasicrystal, the locations of the atomic surfaces, n_0, n_1 and bc_1, are special points with the site symmetry $\bar{5}\bar{3}m$. The thermal tensor $\boldsymbol{B}_j$ can be considered to be approximately isotropic. Hence, the temperature factor is expressed as

$$T_j(\boldsymbol{g}^{\mathrm{par}}, \boldsymbol{g}^{\mathrm{perp}}) = \exp\left\{-\tfrac{1}{4}(B_j^{\mathrm{par}} g^{\mathrm{par}^2} + B_j^{\mathrm{perp}} g^{\mathrm{perp}^2})\right\}. \tag{6}$$

In equation (5), $f_j(g)$ is the atomic scattering factor of the jth atom in the superspace unit cell. The geometrical form factor can be written as

$$q_j(\boldsymbol{g}^{\mathrm{perp}}) = (1/\Omega^{\mathrm{perp}}) \int_{A_j} \exp(2\pi \mathrm{i} \boldsymbol{g}^{\mathrm{perp}} \cdot \boldsymbol{r}^{\mathrm{perp}}) \, \mathrm{d}\boldsymbol{r}^{\mathrm{perp}}. \tag{7}$$

Here, Ω^{perp} and Ω^{par} are the volumes of the 6D unit cell in the perpendicular and parallel subspaces, respectively, and A_j denotes the jth atomic surface. The structure factor represents the scattering power of the quasicrystal within Ω^{par}. Hence, we have

$$S(\boldsymbol{g})/V = F_g/\Omega^{\mathrm{par}} = \pi U_g. \tag{8}$$

It is seen from the previous equations that the diffraction intensity depends on the shapes of the atomic surfaces, as shown in the integration of equation (7).

3.2. Continuous parameterization of the shape of the atomic surface

The approach of Elcoro *et al* [3, 4], in which the shape of the atomic surface is described by surface harmonic expansion, offers an easy way to describe the shape of the atomic surface with continuous parameters and to subsequently refine the parameters. According to Elcoro *et al* [3, 4], the radial functions $r^{\mathrm{ex}}(\theta, \phi)$ and $r^{\mathrm{in}}(\theta, \phi)$, which define the external and internal boundaries of the atomic surface, can be described in terms of linear combinations of ortho-normalized surface harmonics, $Z_l(\theta, \phi)$, which are invariant for the atomic surface site symmetry. The functions $Z_l(\theta, \phi)$ are chosen within the subspace generated by the spherical harmonics $Y_l^m(\theta, \phi)$ with a fixed index l. Thus

$$r(\theta, \phi) = \sum_l a_l Z_l(\theta, \phi) = \sum_l a_l \left(\sum_{m=-l}^{l} z_{lm} Y_l^m(\theta, \phi) \right). \tag{9}$$

The coefficients z_{lm} are determined by the site symmetry of the atomic surface and the normalization condition of the functions $Z_l(\theta, \phi)$. The superspace group $F\bar{5}\bar{3}m$ is normally

assumed for the icosahedral AlPdMn phase. The point symmetries in the parallel and perpendicular spaces are both $\bar{5}\bar{3}m$. The 6D face-centred hypercubic (FCC) direct lattice can be considered as resulting from the ordering on the primitive lattice with the 6D lattice constant $a_P = a_F/2$. The sites n_0, n_1 and bc_1 of the spherical model are either at the vertex or at the body centre. The site symmetries of n_0, n_1 and bc_1 are all $\bar{5}\bar{3}m$. For this site symmetry, a_l can have non-zero values only for $l = 0$, 6, 10, 12, 16 when l is less than or equal to 16. Then $r(\theta, \phi)$ can be expressed as

$$r(\theta,\phi) = a_0 Y_0^0(\theta,\phi) + a_6\left\{\frac{\sqrt{11}}{5}Y_6^0(\theta,\phi) + \frac{\sqrt{7}}{5}[Y_6^5(\theta,\phi) + Y_6^{-5}(\theta,\phi)]\right\} + a_{10}\{\cdots\} + \cdots. \tag{10}$$

The first term, $a_0 Y_0^0(\theta,\phi) = a_0/(4\pi)^{1/2}$, represents a spherical surface with a radius of $a_0/(4\pi)^{1/2}$. To reduce the number of adjustable parameters, and also to save computing time, only the first two coefficients for each boundary, a_0 and a_6, were refined.

3.3. Refinement

We used the QCBED systematic row method [5]. The best fit of the calculated intensity curve to the experimental curve is reached by using the simplex algorithm of optimization. The object function is defined as

$$\chi^2 = \frac{1}{n}\sum_{i,j}\frac{1}{\sigma_{ij}^2}(I_{i,j}^{\exp} - cI_{i,j}^{\mathrm{calc}})^2 + w_c\frac{\sum_m (c_m^{\exp} - c_m^{\mathrm{calc}})^2}{\sum_m (c_m^{\exp})^2} + w_\rho\frac{(\rho^{\exp} - \rho^{\mathrm{calc}})^2}{(\rho^{\exp})^2} + \Delta. \tag{11}$$

Here, i, j are the sequential number of scanned lines and the sequential number of data points in each lines, respectively, n is the total number of data points, I represents the intensity, the superscripts exp and calc stand for experimental and calculated data, respectively, c is a scaling constant, c_m is the relative atomic composition of the mth atom, ρ is the mass density, w_c and w_ρ are the weight parameters for controlling the strength of the restraints with respect to atomic composition and mass density, respectively, and σ_i^2 is the variance of the ith intensity and equals $I^{\exp}$, assuming Poisson statistics. Another term, Δ, is included in the object function to minimize the number of unphysically short interatomic distances. The distances between any two atoms are calculated in each refinement cycle by using the cut method. When the calculated interatomic distance is smaller than the sum of the radii of the two atoms, Δ takes a non-zero positive value. The shorter the distance, the larger the value of Δ. The adjustable parameters include the parameters a_l that describe the shapes of atomic surfaces, thermal parameters B, the beam direction, and the thickness of the specimen.

In the refinement, the 200 beams that were included in the calculations of the diffraction intensities were selected by using the perturbation strength criterion $|U_h/2KS_h|_{\min}$ [10]. Each digit of the index of a 6D reciprocal vector $(n_1\ n_2\ n_3\ n_4\ n_5\ n_6)$ took a value from -20 to 20 in turn, to avoid missing any significant beams. Among the 200 beams, about 50 strong beams were included in the diagonalization of equation (2) and the effects of the remainder were included by introducing the effective Bethe potential [8]. The beams, which correspond to the diffraction lines appearing in the CBED pattern, were among the 50 beams. The additional beams were selected from the 200 beams by using the criteria of Birkeland *et al* [11]. For any beam $\boldsymbol{g}$ in the set of strong beams which are to be diagonalized, if beam $\boldsymbol{h}$ satisfies

$$\Delta U_{g[h]} = U_{g-h}U_h/2KS_hU_g \geqslant B_{\max}, \tag{12}$$

then the beam $\boldsymbol{h}$ must belong to the strong beam set. For any beam $\boldsymbol{g}'$ whose diffraction line appears in the transmitted disk of the CBED pattern, if beam $\boldsymbol{h}$ satisfies $\Delta U_{g'[h]} \geqslant P_{\max}$ then

Table 1. A comparison of the main features of the atomic surfaces from the best fit of the CBED pattern to the spherical model of Boudard *et al* [1]. Here, a_F is the edge length of the 6D face-centred cubic lattice unit cell in direct space; a_0 and a_6 are the coefficients in (9) and (10).

		Spherical model [1]	Best fit of the CBED pattern	
Site	Boundary	Radius	$a_0/\sqrt{4\pi}$	$a_6/\sqrt{4\pi}$
n_0	B1	$0.415a_F$	$0.418a_F$	$0.007\,07a_F$
n_0	B2	$0.63a_F$	$0.624a_F$	$0.075\,1a_F$
n_0	B3	$0.775a_F$	$0.797a_F$	$0.017\,9a_F$
n_1	B4	$0.26a_F$	$0.268a_F$	$-0.017\,9a_F$
n_1	B5	$0.82a_F$	$0.794a_F$	$-0.089\,4a_F$
bc_1	B6	$0.355a_F$	$0.368a_F$	$0.008\,67a_F$

the beam $\boldsymbol{h}$ also belongs to the set of beams that are to be diagonalized. The values of the constants B_{max} and P_{max} are adjusted to keep the number of beams to be diagonalized to about 50, and P_{max} takes a value of 10% of B_{max}.

The spherical model of Boudard *et al* [1] is used as the starting point for the refinement. In the present refinement, the boundaries of the atomic surfaces are described by the surface harmonics of equation (10). Thus, the initial value of a_0 in equation (10) takes the value of $\sqrt{4\pi}$ times the radius of the corresponding sphere in the spherical model [1], and the initial values of $a_6, a_{10}, \ldots$ in equation (10) take the value zero. It is assumed that, for two adjacent shells, the external boundary of the inner shell is exactly the internal boundary of the outer shell, which is similar to the spherical model [1]. The chemical order of the spherical model of Boudard *et al* [1] was determined using neutron diffraction and anomalous x-ray diffraction. This chemical order is used in the present refinement. The $Al_{70.5}Pd_{21}Mn_{8.5}$ icosahedral phase has a face-centred hypercubic lattice with a lattice constant of $a_F = 1.2902$ nm in the six-dimensional direct space. The radii of the spherical boundaries of the atomic surfaces in this model are listed in table 1. The experimental mass density used in the refinement is 5.18 g cm^{-3}.

The coordinate system proposed by Cahn *et al* [12] is used in this paper. The corresponding six-dimensional rotation matrix used is then

$$\frac{1}{\sqrt{2(2+\tau)}}\begin{bmatrix} 1 & \tau & 0 & -1 & \tau & 0 \\ \tau & 0 & 1 & \tau & 0 & -1 \\ 0 & 1 & \tau & 0 & -1 & \tau \\ -\tau & 1 & 0 & \tau & 1 & 0 \\ 1 & 0 & -\tau & 1 & 0 & \tau \\ 0 & -\tau & 1 & 0 & \tau & 1 \end{bmatrix}. \tag{13}$$

4. Results and discussion

Figure 1 shows the transmitted disk of the CBED pattern. The diffraction lines are indexed by matching the experimental pattern to a computer-simulated diffraction line pattern on the basis of kinematic theory. Figure 2(a) shows the experimental energy filtered CBED pattern in the $(\bar{6}\bar{2}\bar{2}\bar{4}\bar{2}4)$ systematic reflection condition. The data scanned along lines 3 and 5 were used in the refinement. Figure 2(b) shows the line profile of line scan 3, the calculated intensities, and the differences between the calculated and experimental intensities. The structure parameters obtained from the best fit of the calculated to the experimental line profile are listed in table 1 to compare these parameters with those of the spherical model. The boundaries that define the atomic surfaces are shown in figure 3. The central sections of the atomic surfaces in the Y–Z plane through n_0, n_1, bc_1 points, respectively, are shown in figure 4.

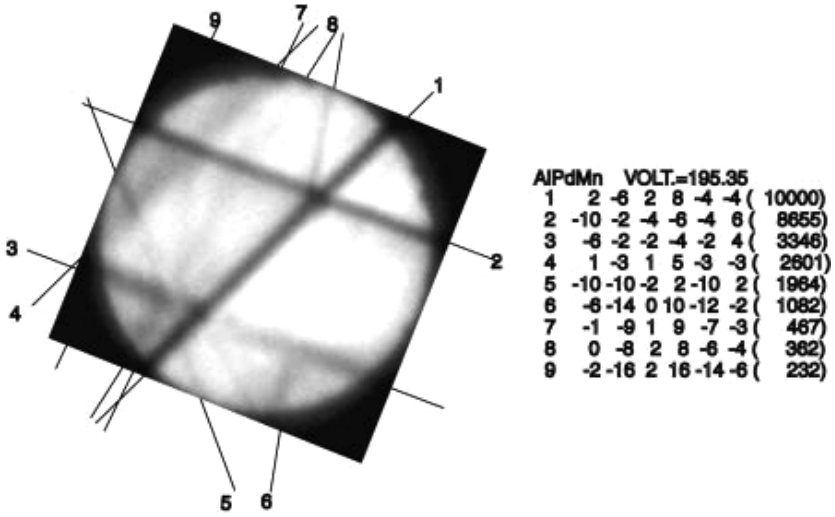

Figure 1. Diffraction lines in the transmitted disk of the CBED pattern and the indexes for each diffraction lines. The values in the parentheses following the indexes are the intensities of the diffraction beams calculated in kinematic approximation.

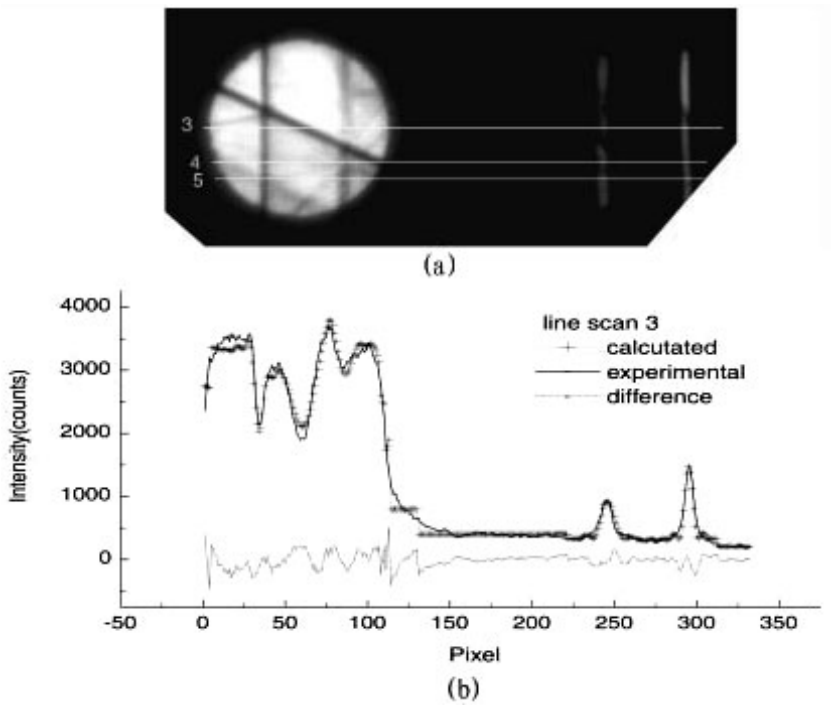

Figure 2. (a) The experimental CBED pattern in the $(\bar{6}\bar{2}\bar{2}\bar{4}\bar{2}4)$ systematic reflection condition. (b) The experimental line profile and the best fits for line scan 3. The differences between the calculated and experimental intensities are shown by the dotted curve.

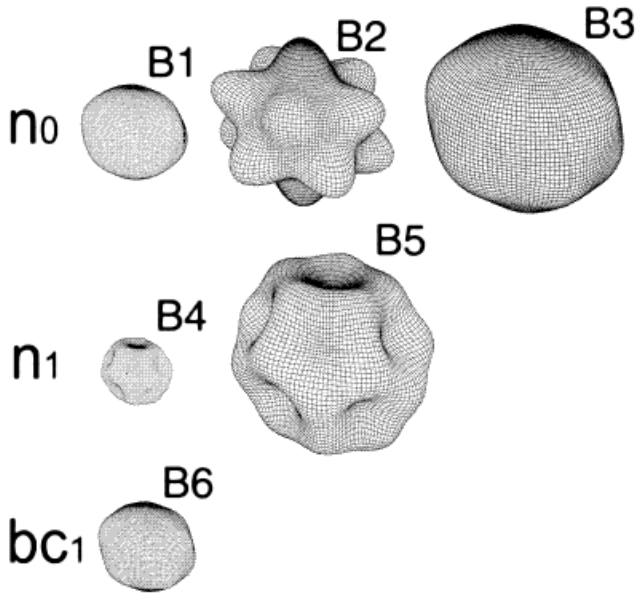

Figure 3. The boundaries obtained for the atomic surfaces of the AlPdMn icosahedral phase.

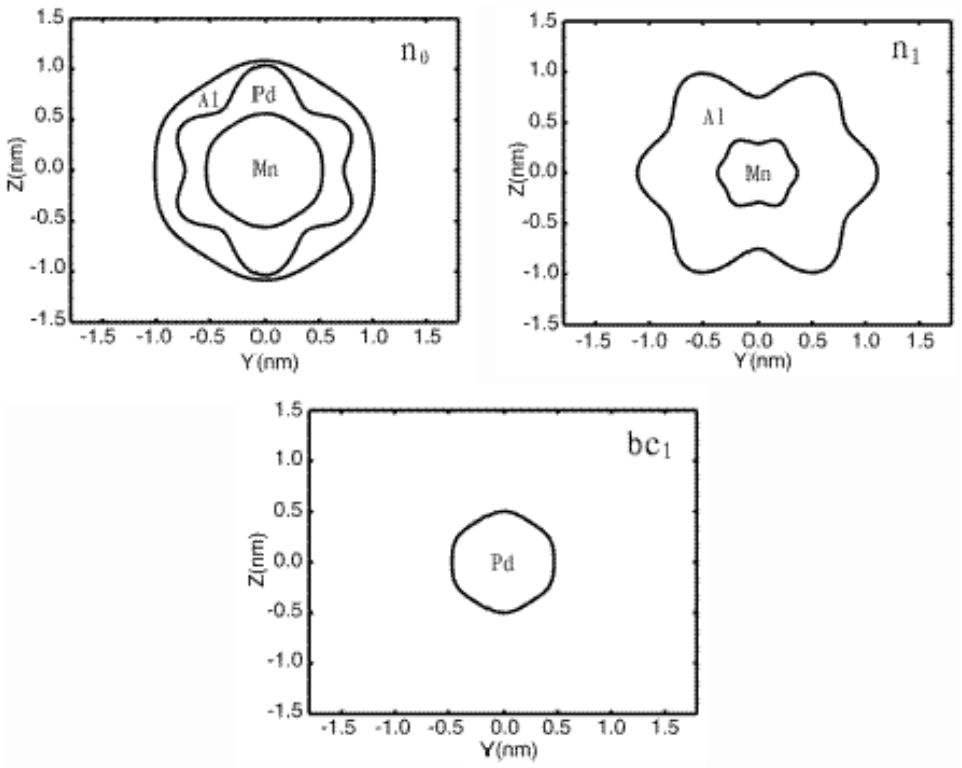

Figure 4. The central sections of the atomic surfaces at n_0, n_1 and bc_1 on the Y–Z plane.

Table 2. Statistics on unphysically short interatomic distances in the present model. The parameter r is the ratio of the calculated interatomic distance d_{ij} (from atom i to its neighbour j) to the sum of the radii of the two atoms, $r_i + r_j$, i.e. $r = d_{ij}/(r_i + r_j)$. Here, the metallic radii, $r_{\mathrm{Al}} = 0.142$ nm, $r_{\mathrm{Pd}} = 0.137$ nm and $r_{\mathrm{Mn}} = 0.136$ nm were used.

	Percentage of atoms whose r lies in the range in the first column (%)	
r	Present model	Spherical model
$\geqslant 1.0$	2.06	0.266
1.0–0.9	93.5	92.6
0.9–0.8	0.00	0.00
0.8–0.7	0.00	0.00
0.7–0.6	3.93	4.67
0.6–0.5	0.00	0.00
0.5–0.4	0.00	0.00
0.4–0.3	0.525	2.49
0.3–0	0.00	0.00

It is seen from table 1 and figures 3 and 4 that the irregularity of the atomic surface at n_0 for Pd obtained from fitting CBED is in agreement qualitatively with the prediction from anomalous x-ray scattering studies [2]. Nevertheless, the geometric fluctuation of about 0.2 nm around the sphere is slightly larger than the value of 0.12 nm [2]. The shapes of the atomic surfaces at n_0 and n_1 for Al are also changed significantly from the sphere. However, the shapes of the atomic surfaces for Mn are mainly spherical, with very little fluctuation, and the sizes of the spheres are nearly the same as those of Boudard's spherical model [1].

We calculated the interatomic distances for the atoms within a 7 nm $\times$ 7 nm $\times$ 7 nm box and used some simple statistics. The total number of atoms is 23 258, which includes 16 077 Al atoms, 5151 Pd atoms and 2030 Mn atoms. The calculated mass density is 5.15 g cm^{-3}. The main results are shown in table 2. The parameter r is defined as the ratio of the calculated interatomic distance d_{ij} (from atom i to its neighbour j) to the sum of the radii of the two atoms, $r_i + r_j$, i.e. $r = d_{ij}/(r_i + r_j)$. The metallic radii $r_{\mathrm{Al}} = 0.142$ nm, $r_{\mathrm{Pd}} = 0.137$ nm, and $r_{\mathrm{Mn}} = 0.136$ nm from [13] were used here. It is seen that the percentage of atoms that have unphysically short interatomic distance to their neighbours is reduced by using surface harmonics in describing the shape of the atomic surface and by adding the term Δ to the object function in the refinement of the QCBED technique.

Table 3 lists the thermal parameter components B^{par} obtained from fitting the calculated line profile to the experimental line profile. It is seen that, due to the fact that the CBED experiments were performed at lower temperature, the values of the thermal parameter B^{par} obtained in the present refinement are smaller than those in [2]. It is also seen that the value of B^{par} for Al is larger than those for Mn and Pd, which implies that the amplitude of the thermal vibration of Al atoms in the quasicrystal is larger than those of the other two types of atoms.

Using the parameters obtained for the atomic surface boundaries, the three-dimensional structure of the AlPdMn icosahedral phase is generated by using the cut method. The origin of the superspace is located successively at the six-dimensional lattice nodes n_0, n_1 and bc_1. Figures 5 and 6 show the shells of the cluster whose centre corresponds to the six-dimensional lattice nodes n_0 and n_1, respectively. The number of atoms, the radius r of polyhedron, and the ratio of r to $a_{3\mathrm{D}}$, where $a_{3\mathrm{D}} = a_{\mathrm{P}}/\sqrt{2} = 0.4561$ nm, for each shell are listed in table 4. The type of shell and the ratio $r/a_{3\mathrm{D}}$ of the extended Mackay cluster (proposed by Duneau [14]) are also listed in table 4. It is seen that, for the cluster with a centre corresponding to n_0, the first six

Table 3. Column 5 lists the values of the thermal parameter component B^{par}, as defined in equation (5), that were obtained by fitting the CBED pattern. The CBED experiment was performed with a liquid nitrogen cooled specimen holder. For comparison, the values of B^{par} and B^{perp} given in [1, 2] are also listed in the table. It is noted that the parameters B^{par} and B^{perp} in [1, 2] are defined with $\exp\{-(B^{\mathrm{par}}Q_{\mathrm{par}}^2 + B^{\mathrm{perp}}Q_{\mathrm{perp}}^2)\}$ and $Q_{\mathrm{par}} = 2\pi/d_{\mathrm{par}}$, where d_{par} is the spacing of the atomic plane. The values of B^{par} and B^{perp} shown in this table are $(4\pi)^2$ times 0.000 044 nm^2 and 0.007 nm^2 [2], respectively.

		Spherical model [1]		The best fit of CBED pattern
Site	Atom	B^{par} (nm^2)	B^{perp} (nm^2)	B^{par} (nm^2)
n_0	Mn (within B1)	0.0069	1.1	0.000 469
n_0	Pd (between B1 and B2)	0.0069	1.1	0.000 499
n_0	Al (between B2 and B3)	0.0069	1.1	0.001 45
n_1	Mn (within B4)	0.0069	1.1	0.000 566
n_1	Al (between B4 and B5)	0.0069	1.1	0.001 20
bc_1	Pd (within B6)	0.0069	1.1	0.000 434

shells, including one Mn atom located at the centre, are coincident with the extended Mackay cluster with respect to the type of polyhedron and the ratio of r to $a_{3\mathrm{D}}$. Nevertheless, the vertices in the present model are all occupied either by Al atoms or by Mn atoms (icosidodecahedron with $r/a_{3\mathrm{D}} = 1.701$), and the icosahedral symmetry of the cluster is maintained. For the cluster with a centre corresponding to n_1, the 12 Mn atoms (icosahedron), the 30 Al atoms (icosidodecahedron), the 60 Al atoms (rhombicosidodecahedron) and the larger 30 Al atoms (icosidodecahedron) are also in the shell series of the extended Mackay cluster. However, the dodecahedron with $r/a_{3\mathrm{D}} = 0.563$ in the shell series of the extended Mackay cluster does not appear in the shell series of a cluster with a centre located at n_1, shown in figure 6. It is noted that the 12 Pd icosahedron with $r/a_{3\mathrm{D}} = 1.618$ in the cluster with a centre at n_0 belongs to the shell series of the extended Bergman cluster [14] rather than the shell series of the extended Mackay cluster. The 20 Pd dodecahedron with $r/a_{3\mathrm{D}} = 1.473$ in the cluster with a centre at n_1 also belongs to the shell series of the extended Bergman cluster.

The shells of the cluster with a centre corresponding to the six-dimensional lattice node bc_1 are shown in figure 7. The features of the shells are listed in table 5. It is seen that the first four shells belong to the shell series of the extended Bergman cluster [14]. However, two incomplete truncated icosahedrons with an $r/a_{3\mathrm{D}}$ of 1.220 and 1.391 do not appear in the shells shown in figure 7.

In the pseudo-Mackay icosahedron model of Boudard *et al* [1] the cluster contains 51 atoms. The internal shell is a body-centred cubic of nine Al atoms, and the cubic can be considered to be part of a dodecahedron. The second shell is a icosahedron occupied by Mn atoms plus a small number of Al or Pd atoms, and the external icosidodecahedron is made of Al atoms alone or of Al plus Pd atoms, depending on which node, n_0 or n_1, the centre of the cluster is sited. According to electronic structure calculations [15], this clustered structure corresponds to a stable low-energy state. Recently, a number of theoretical investigations [14, 16, 17] showed that the Bergman clusters are the basic dominant elements for the icosahedral AlPdMn (i-AlPdMn) phase. The discrepancy is noted between the present result and the existing models of theoretical and experimental investigations. To increase the reliability of the structure refinement using QCBED, work is in progress to investigate using different algorithms of optimization, as well as to investigate refining simultaneously several CBED patterns, in each of which one or more specified strong reflections are excited.

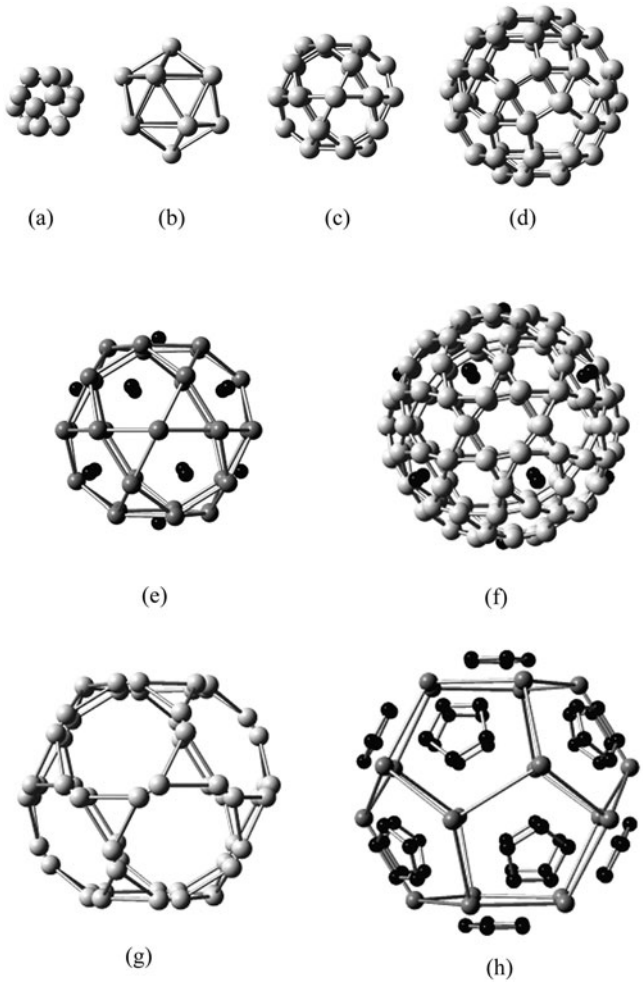

Figure 5. Shells of the cluster with a centre located at the six-dimensional lattice node n_0. The light grey balls with the largest size represent Al atoms, the small black balls represent Pd, and the darker balls with intermediate size represent Mn.

5. Summary

In this paper the QCBED technique is used in the refinement of the atomic structure of icosahedral AlPdMn quasicrystals by fitting the experimental line scan profile to calculated intensities by means of the dynamic theory of electron diffraction. The shapes of the atomic surfaces' boundaries are described using a truncated series of surface harmonics, and the coefficients in the surface harmonic expansion are refined, together with the thermal parameters, thickness of the sample etc. The refined parameters, which describe the shapes of the atomic surfaces' boundaries, show that the fluctuation in the external boundary of the atomic surface for Pd at the site n_0 can be as large as 0.2 nm. The fluctuations in the internal boundary at n_0 and the external boundary at n_1 of the atomic surfaces for Al are also significant. The shapes of the atomic surfaces for Mn remain essentially spherical. Compared to the spherical model, the percentage of unphysically short interatomic distances is reduced. The thermal parameter

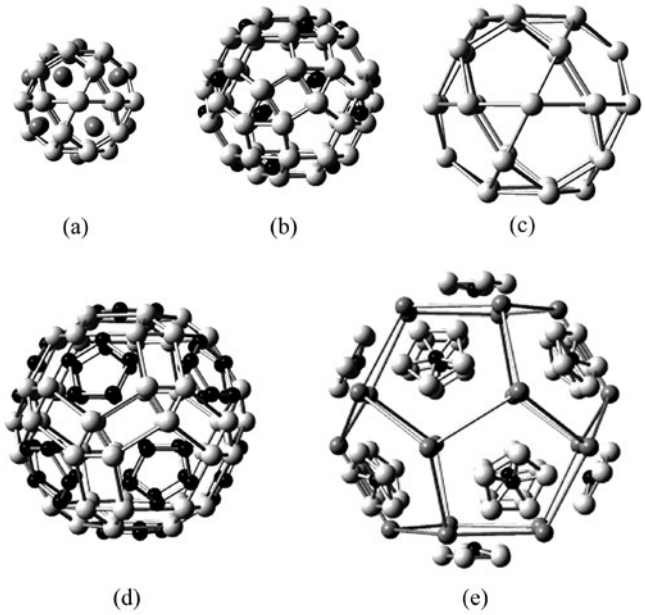

Figure 6. Shells of the cluster with a centre located at the six-dimensional lattice node n_1. The light grey balls with the largest size represent Al atoms, the small black balls represent Pd, and the darker balls with intermediate size represent Mn.

Table 4. The first four columns and the second four columns list the number of atoms, radius and the ratio r/a_{3D} for each shell of the cluster corresponding to the six-dimensional lattice nodes n_0 and n_1, respectively. The type of shell and the ratio r/a_{3D} of the extended Mackay cluster [14] are listed in the 9th and 10th columns.

Cluster with centre corresponding to n_0				Cluster with centre corresponding to n_1				Extended MC [14]	
Figure	No of atoms	Radius r (nm)	r/a_{3D}	Figure	No of atoms	Radius r (nm)	r/a_{3D}	Shell	r/a_{3D}
	1 Mn	0	0		1 Mn	0	0	1	0
5(a)	20 Al	0.2567	0.563					20	0.563
5(b)	12 Al	0.4561	1	6(a)	12 Mn	0.4561	1	12	1
5(c)	30 Al	0.4796	1.051		30 Al	0.4796	1.051	30	1.051
5(d)	60 Al	0.6619	1.451	6(b)	60 Al	0.6619	1.451	60	1.451
					20 Pd	0.6721	1.473		
5(e)	12 Pd	0.7381	1.618						
	30 Mn	0.7761	1.701	6(c)	30 Al	0.7761	1.701	30	1.701
5(f)	60 Al	0.9002	1.974	6(d)	60 Pd	0.9002	1.974		
	60 Al	0.9123	2.000		60 Al	0.9123	2.000		
	12 Pd	0.9123	2.000						
5(g)	60 Al	1.0200	2.236	6(e)	12 Pd	1.0200	2.236		
5(h)	20 Mn	1.0875	2.384		20 Mn	1.0875	2.384		
	60 Pd	1.0975	2.406		60 Al	1.0975	2.406		

components B^{par} obtained at low temperature show that the thermal parameters of Al are much larger than the parameters of Pd and Mn. Using the cut method, clusters are obtained with a centre sited successively at the six-dimensional lattice nodes n_0, n_1 and bc_1. The clusters with

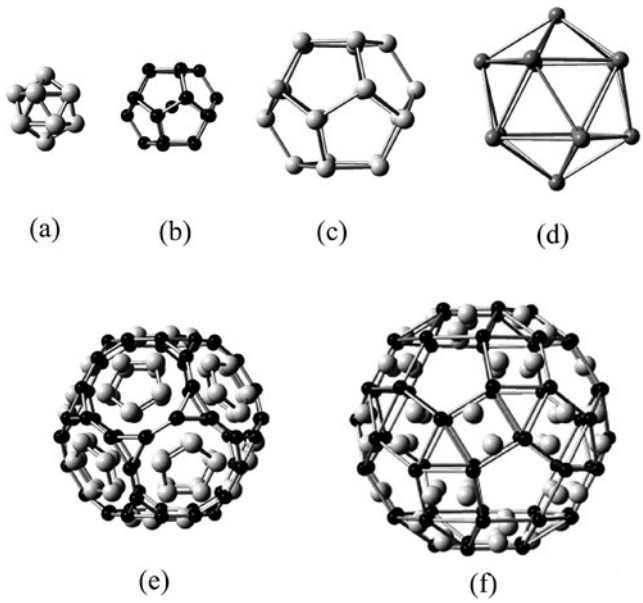

Figure 7. The shells of the cluster with a centre located at the six-dimensional lattice node bc_1. The light grey balls with the largest size represent Al atoms, the small black balls represent Pd, and the darker balls with intermediate size represent Mn.

Table 5. The first four columns list the number of atoms, radius and the ratio r/a_{3D} for each shell of the cluster corresponding to the six-dimensional lattice node bc_1. The type of shell and the ratio r/a_{3D} of the extended Bergman cluster [14] are listed in the 5th and 6th column.

Cluster with centre corresponding to bc_1				Extended Bergman cluster [14]	
Figure	No of atoms	Radius r (nm)	r/a_{3D}	Shell	r/a_{3D}
	1 Mn	0	0		
7(a)	12 Al	0.2819	0.618	12	0.618
7(b)	20 Pd	0.4154	0.911	20	0.911
				60	1.220
				60	1.391
7(c)	20 Al	0.6721	1.473	20	1.473
7(d)	12 Mn	0.7381	1.618	12	1.618
7(e)	60 Al	0.8257	1.810		
	60 Pd	0.8802	1.930		
7(f)	60 Al	1.0266	2.251		
	60 Pd	1.0710	2.348		

a centre corresponding to the 6D lattice nodes n_0 and n_1 show predominantly the features of the extended Mackay cluster, while the clusters with a centre corresponding to the 6D lattice node bc_1 show mainly the features of the extended Bergman cluster.

Acknowledgments

We are very grateful to Dr J M Zuo for providing the source code of his program REFINE_CB5 for the structure factor refinement of crystals, and to Dr L Elcoro for providing the source code

of his program QUASI. We also want to thank Professor K Urban for providing the icosahedral AlPdMn quasicrystal specimens. This work was supported financially by the National Natural Science Foundation of China (no 59871034).

References

[1] Boudard M, de Boissieu M, Janot C, Heger G, Beeli C, Nissen H-U, Vincent H, Ibberson R, Audier M and Dubois J M 1992 *J. Phys.: Condens. Matter* **4** 10149
[2] de Boissieu M, Stephens P, Boudard M, Janot C, Chapman D L and Audier M 1994 *J. Phys.: Condens. Matter* **6** 10725
[3] Elcoro L, Perez-Mato J M and Madariaga G 1994 *Acta Crystallogr.* A **50** 182
[4] Elcoro L and Perez-Mato J M 1994 *Acta Crystallogr.* B **50** 294
[5] Zuo J M and Spence J C H 1991 *Ultramicroscopy* **35** 185
[6] Tanaka M, Terauchi M and Tsuda K 1994 *Convergent Beam Electron Diffraction* vol 3 (Tokyo: JEOL)
[7] Cheng Y and Wang R 1989 *Phys. Status Solidi* b **152** 33
[8] Spence J C H and Zuo J M 1992 *Electron Microdiffraction* (New York: Plenum)
[9] Steurer W and Haibach T 1999 *Physical Properties of Quasicrystals* ed Z M Stadnik (Berlin: Springer) p 51
[10] Zuo J M and Weickenmeier A L 1995 *Ultramicroscopy* **57** 375
[11] Birkeland C, Holmestad R, Marthinsen K and Høier R 1996 *Ultramicroscopy* **66** 89
[12] Cahn J W, Shechtman D and Gradias D 1986 *J. Mater. Res.* **1** 13
[13] Evans R C 1976 *An Introduction to Crystal Chemistry* (London: Cambridge University Press)
[14] Duneau M 2000 *Mater. Sci. Eng.* **294–296** 192
[15] Janot C 1997 *J. Phys.: Condens. Matter* **9** 1493
[16] Quandt A and Elser V 2000 *Phys. Rev.* B **61** 9336
[17] Gratias D, Puyraimond F, Quiquandon M and Katz A 2000 *Phys. Rev.* B **63** 024202-1